
THE LITTLE W-NET THAT COULD: STATE-OF-THE-ART RETINAL VESSEL SEGMENTATION WITH MINIMALISTIC MODELS

PREPRINT - UNDER REVIEW

Adrian Galdran^{1,*}, André Anjos², José Dolz³, Hadi Chakor⁴, Hervé Lombaert³, Ismail Ben Ayed^{3,5}

¹University of Bournemouth, UK ²IDIAP Research Institute, Switzerland

³École de Technologie Supérieure de Montréal, Canada ⁴Diagnos Inc., Canada

⁵CRCHUM University of Montreal Hospital Centre

* Corresponding author: agaldran@bournemouth.ac.uk

September 7, 2020

ABSTRACT

The segmentation of the retinal vasculature from eye fundus images represents one of the most fundamental tasks in retinal image analysis. Over recent years, increasingly complex approaches based on sophisticated Convolutional Neural Network architectures have been slowly pushing performance on well-established benchmark datasets. In this paper, we take a step back and analyze the real need of such complexity. Specifically, we demonstrate that a minimalistic version of a standard U-Net with several orders of magnitude less parameters, carefully trained and rigorously evaluated, closely approximates the performance of current best techniques. In addition, we propose a simple extension, dubbed W-Net, which reaches outstanding performance on several popular datasets, still using orders of magnitude less learnable weights than any previously published approach. Furthermore, we provide the most comprehensive cross-dataset performance analysis to date, involving up to 10 different databases. Our analysis demonstrates that the retinal vessel segmentation problem is far from solved when considering test images that differ substantially from the training data, and that this task represents an ideal scenario for the exploration of domain adaptation techniques. In this context, we experiment with a simple self-labeling strategy that allows us to moderately enhance cross-dataset performance, indicating that there is still much room for improvement in this area. Finally, we also test our approach on the Artery/Vein segmentation problem, where we again achieve results well-aligned with the state-of-the-art, at a fraction of the model complexity in recent literature. All the code to reproduce the results in this paper is released.

Keywords one, two, three, four

1 Introduction and Related Work

Retinal vessel segmentation is one of the first and most important tasks in for the computational analysis of eye fundus images. It represents a stepping stone for more advanced applications like artery/vein ratio computation [11], blood flow analysis [5], image quality assessment [12], retinal image registration [13], or retinal image synthesis [14].

Initial approaches to retinal vessel segmentation were fully unsupervised and relied on conventional image processing operations like mathematical morphology [15,16]

or adapted edge detection operations [17]. The idea behind these methods is to apply some kind of transformation to a retinal image so that vessel intensities are emphasized, and then threshold the result to achieve a segmentation. Although research on advanced filtering techniques for retinal vessel segmentation has continued over more recent years [6, 18], these kind of techniques consistently reach lower performance on established benchmarks, likely due to their inability to handle images with pathological structures and generalizing to images with different appearances and resolutions.

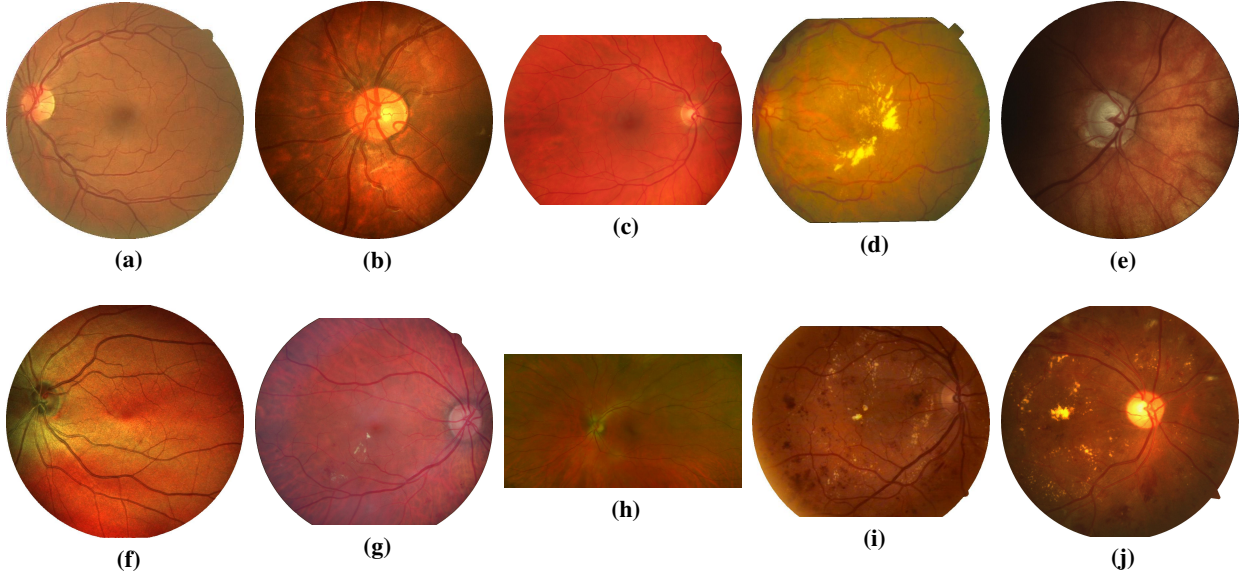


Figure 1: This work provides the most comprehensive cross-dataset performance study on vessel segmentation to date. A representative image from each of the 10 databases considered in this paper: DRIVE [1], CHASE-DB 1 [2], HRF [3], STARE [4], LES-AV [5], IOSTAR [6], DR HAGIS [7], AV-WIDE [8], DRIDB [9], UoA-DR [10]. A detailed description of each database is given in Table 2.

In contrast, early learning-based approaches quickly showed more promising results and better performance than their image processing counterparts [1, 19–22]. The common strategy of these techniques consisted on the extraction of specifically designed local descriptors that were later passed to a relatively simple classifier, and the focus became to derive the most discriminative visual features for the task at hand.

This predominance of machine learning techniques was reinforced with the emergence of deep neural networks. After initial realization that Convolutional Neural Networks (CNNs) could outperform previous methods, bypassing any manual feature engineering and directly learning from raw data [23, 24], a constant stream of publications has kept appearing on this topic, up to the point that almost any new competitive vessel segmentation technique is based now on this approach.

Standard CNN approaches to retinal vessel segmentation are based on the sequential application of a stack of convolutional layers that subsequently downsample and up-sample input images to reach a probabilistic prediction of vessel locations. The weights of the network are then iteratively updated to improve those predictions by means of the minimization of a given miss-classification loss, *e.g.* cross-entropy. Either processing small image patches [23] or the entire image [24], these approaches can succeed in segmenting the retinal vasculature with few annotated training data.

Extensions to the above paradigm tend to involve complex operations, like specifically designed network lay-

ers. Fu *et al.* introduced a Conditional Random Field recurrent layer to model more global relationships between pixels [25], and Shi *et al.* combined convolutional and graph-convolutional layers to better capture global vessel connectivity [26]. Guo *et al.* introduced dense dilated layers that adjust the dilation rate based on vessel thickness [27], and Fan *et al.* proposed a multi-frequency convolutional layer (OctConv) in [28]. Other custom convolutional blocks and layers based on domain knowledge have been explored in several recent works [29, 30].

Non-standard losses have also been proposed in recent years. Yan *et al.* [31] trained a U-Net architecture [32] by minimizing a joint-loss that receives output predictions from two separate network branches, one with a pixel-level and one with a segment-wise loss. The same authors introduced a similar segment-level approach in [33], whereas Mou *et al.* employed a multi-scale Dice loss [34], Zhao *et al.* proposed a combination of global pixel-level loss and local matting loss [35], and Zhang and Chung introduced in [36] a deeply supervised approach in which various loss values extracted at different stages of a CNN are combined and backpropagated, with artificial labels in vessel borders turning the problem into a multi-class segmentation task. Generative Adversarial Networks have also been proposed for retinal vessel segmentation [37–40], although without achieving widespread popularity due to the difficulty in training these techniques.

It is also worth reviewing efficient approaches to retinal vessel segmentation, as we plan to introduce in this paper high-performance lightweight models. These meth-

ods typically appear in works focused on retinal vessel segmentations for embedded/mobile devices. In this context, conventional unsupervised approaches are still predominant. Arguello *et al.* employ image filtering coupled with contour tracing [41], Bibiloni *et al.* apply simple hysteresis thresholding [42], whereas Xu *et al.* adapt Gabor filters and morphological operations for vessel segmentation in smartphone devices [43]. Only recently, Laibacher *et al.* have explored efficient CNN architectures specifically designed for vessel segmentation on eye fundus images [44]. Their proposed M2U-Net architecture leverages an ImageNet-pretrained MobileNet model [45] and achieves results slightly inferior to the state-of-the-art.

1.1 Goals and Contributions

The goal of this paper is to show that 1) as recently shown in other computer vision problems [46, 47], there is no need of designing complex CNN architectures to outperform *most current techniques* on the task of retinal vessel segmentation, and 2) when a state-of-the-art model is trained on a particular dataset and tested on images from different data sources, it can result in poor performance. On our way to establish these two facts, we make several contributions:

1. We introduce a simple extension of the standard U-Net architecture, named W-Net, which allows us to achieve outstanding performance on well-established datasets.
2. We establish a rigorous evaluation protocol, aiming to correct previous pitfalls in the area.
3. We test our approach in a large collection of retinal datasets, consisting of 10 different databases showing a wide range of characteristics, as illustrated in Fig. 1.
4. Our cross-dataset experiments reveal that domain shift can induce performance degradation in this problem. We propose a simple strategy to address this challenge, which is shown to recover part of the lost performance.
5. Finally, we also apply our technique to the related problem of Artery/Vein segmentation from retinal fundus images, matching the performance of previous approaches with models that contain much fewer parameters.

We believe that our results open the door to a more systematic study of new domain adaptation techniques in the area of retinal image analysis: since training one of our models to reach superior performance takes approximately 20 minutes in a single consumer GPU, our work can serve as a first step for quick design and experimentation with improved approaches that can eventually bridge the generalization gap across different data sources revealed by our experiments. To favor research in this direction, we release the code and data to reproduce our results at github.com/agaldran/lwnet.

2 Methodology

2.1 Baseline U-Net: structure and complexity

One of the main goals of this work is to explore the lower limits in model complexity for the task of retinal vessel segmentation. Accordingly, we consider one of the simplest and most popular architectures in the field of medical image segmentation, namely the U-Net [32]. A standard U-Net is a convolutional autoencoder built of a downsampling CNN that progressively applies a set of filters to the input data while reducing its spatial resolution, followed by an upsampling path that recovers the original size. U-Nets typically contain skip connections that link activation volumes from the downsampling path to the upsampling path via concatenation or addition in order to recover higher resolution information and facilitate gradient flow during training.

Let us parametrize a U-Net architecture ϕ by the number of times the resolution is downsampled/upsampled k , and the number of filters applied in each of these depth levels, f_k . To simplify our analysis, we will only consider filters of size 3×3 , and we double the amount of filters each time we increase k - this is a common pattern in U-Net designs. Therefore, in this work a U-Net is fully specified by a pair of numbers (k, f_0) , and we denote it by ϕ_{k, f_0} . In addition, we assume that Batch-Norm layers are inserted after each convolutional operation and that extra skip connections are added within each block. An example of such design pattern is shown in the left hand side of Fig. 2. In the remaining of this work, we will consider the $\phi_{3,8}$ architecture, which contains approximately 34,000 parameters. It is important to stress that this represents 1-3 orders of magnitude less than previously proposed CNNs for the task of retinal vessel segmentation.

2.2 The W-Net architecture

We also introduce a modification of the U-Net architecture, that we refer to as W-Net. The idea behind a W-Net, denoted by Φ , is straightforward: for an input image x , the result of forward-passing it through a standard U-Net $\phi^1(x)$ is concatenated to x , and passed again through a second U-Net, which would be represented as:

$$\Phi(x) = \phi^2(x, \phi^1(x)). \quad (1)$$

In practice, ϕ^1 generates a first prediction of vessels localization that can then be used by ϕ^2 as a sort of attention map to focus more on interesting areas of the image, as shown in Fig. 2. Of course a W-Net Φ contains twice the amount of learnable parameters as a standard U-Net. However, since the base U-Nets $\phi_{3,8}^1, \phi_{3,8}^2$ involved in its definition contain only 34,000 each, the W-Net considered in this paper will have around 68,000 weights, which is still one order of magnitude below the simplest architecture proposed to date for vessel segmentation, and three orders of magnitude smaller than state-of-the-art architectures.

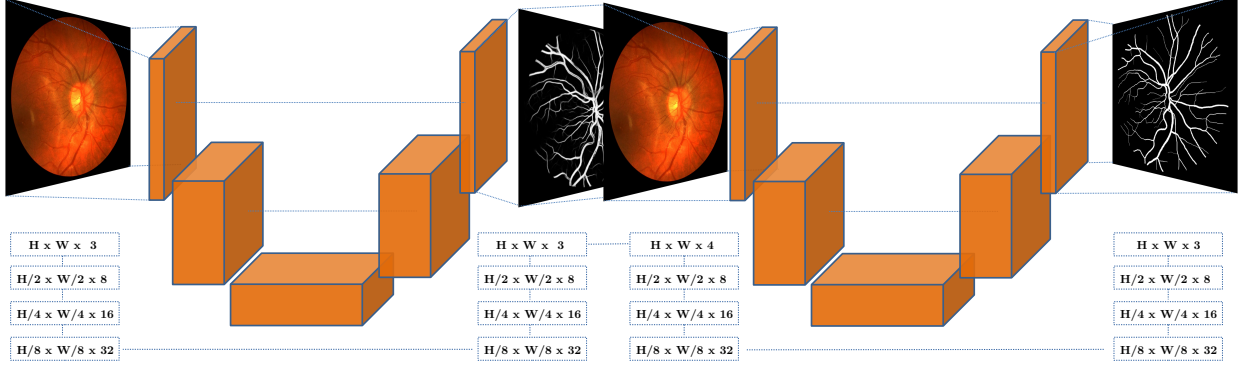


Figure 2: Representation of the WNet architecture. The left-hand-side part of the architecture corresponds to a standard minimal U-Net $\phi_{3,8}$ with $\sim 34K$ parameters, and it achieves performance on-par with the state-of-the-art. The full W-Net, defined by eq. (1), is composed of two consecutive U-Nets; it outperforms all previous approaches with just around 70k parameters: 1-3 orders of magnitude less than previously proposed CNNs.

2.3 Training Protocol

In all the experiments reported in this paper, the training strategy remains the same. Specifically, we minimize a standard cross-entropy loss between the predictions of the model on an image x and the actual labels y . It is worth mentioning that in the W-Net case, an auxiliary loss is computed for the output of the first network and linearly combined with the loss computed for the second network:

$$\mathcal{L}(\Phi(x), y) = \mathcal{L}(\phi^1(x), y) + \mathcal{L}(\phi^2(x), y) \quad (2)$$

The loss is backpropagated and minimized by means of the Adam optimization technique. The learning rate is initially set to $\lambda = 10^{-2}$, and cyclically annealed following a cosine law until it reaches $\lambda = 10^{-8}$. Each cycle runs for 50 epochs, and we adjust the amount of cycles (based on the size of each training set) so that we reach 4000 iterations in every experiment.

Images are all resized to a common resolution and processed with standard data augmentation techniques, and

the batch size is set to 4 in all experiments. During training, at the end of each cycle the Area Under the ROC curve is computed on a separate validation set, and the best performing model is kept. Test-Time-Augmentations (horizontal and vertical image flips) are applied during inference in all our experiments.

2.4 A simple Baseline for Domain Adaptation

One of the main goals in this paper is to show that, even if simple approaches can outperform much more complex current techniques, the problem of retinal vessel segmentation is not as trivial as we may extrapolate from this. The reason is that models trained on a given dataset do not reach the same level of performance when tested on retinal images sampled from markedly different distributions, as we quantitatively show in section 3.3. A relevant drop of performance appears when a model trained on a given source dataset \mathcal{S} is used to generate segmentations on a substantially different target dataset \mathcal{T} .

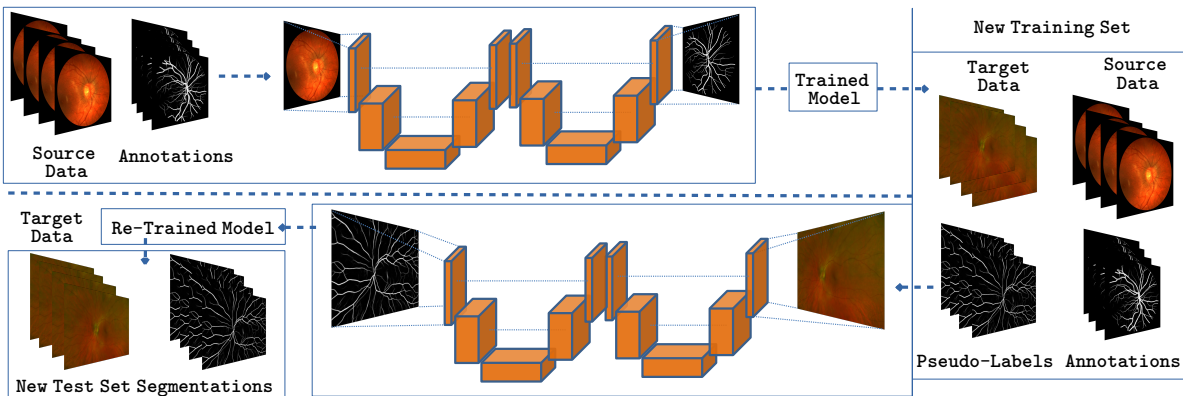


Figure 3: Domain Adaptation strategy employed in this work: A model trained on source data is used to generate pseudo-labels on a target dataset. The original source data and the target data with the pseudo-labels are used to fine-tune that model and produce better predictions.

Attempting to close such performance gap is a task falling within the area of Domain Adaptation, which has been subject of intensive research in the computer vision community for the last years [48]. Here we explore a simple solution to address this challenge in the context of retinal vessel segmentation. Namely, given a model U_S trained on \mathcal{S} we proceed by first generating probabilistic segmentations for each image $x \in \mathcal{T}$. We then merge the source dataset labels y_S with the target dataset segmentations $\{U_S(x) \mid x \in \mathcal{T}\}$, which we treat as pseudo-labels. Lastly, we fine-tune U_S in this new dataset, starting from the weights of the model trained on \mathcal{S} , with a learning rate reduced by a factor of 100, for 10 extra epochs. During training, we monitor the AUC computed in the training set (including both source labels and target pseudo-labels) as a criterion for selecting the best model. It is worth stressing that pseudo-labels $U_S(x)$ remain with probabilistic values in $[0, 1]$, rather than binary, with the goal of informing the model about the uncertainty present on them. The rationale behind this is to force the new model to learn from segmentations in \mathcal{S} with confident annotations, while at the same time exposing it to images from \mathcal{T} before testing on them. A graphical overview of this strategy is shown in Fig. 3.

2.5 Evaluation Protocol

Unfortunately, a rigorous evaluation protocol for retinal vessel segmentation is missing in the literature due to several issues: differences in train/test splits in common benchmarks, or wrongly computed performance metrics. Below we outline what we understand as a correct evaluation procedure:

1. All performance metrics are computed at native image resolution and excluding pixels outside the retinal area, which are trivially predicted as having zero probability of being part of a vessel.
2. Whenever an official train/test split exists, we follow it. When there is none, we follow the least “favorable” split we could find in previous works, *i.e.* the one assigning less images for training. We make this decision based on the low difficulty of the vessel segmentation task; this is in contrast with other works that employ leave-one-out cross-validation, which can use up to 95% of the data for training [31, 49].
3. We first accumulate all probabilities and labels across the training set, then perform AUC analysis and derive an optimal threshold (maximizing the Dice score) to binarize predictions. We then apply the same procedure on the test set, now using the pre-computed threshold to binarize test segmentations. This stands opposed to computing metrics per-image and reporting the mean performance [50], or using a different threshold on each test image for binarizing probabilistic predictions [51].
4. Cross-dataset experiments are reported in a variety of different datasets. No pre-processing or hyper-

parameters are re-adjusted when changing datasets, since this heavily undermines the utility of a method. This is a typical shortcoming of unsupervised approaches, which tend to modify certain parameters to account for different vessel calibers [6]. Also, the threshold to binarize predictions on different datasets is the one derived from the original training set, without using test data to readjust it.

5. We do not report accuracy, since this is a highly imbalanced problem; the Dice score is a more suitable figure of merit. We also report Matthews Correlation Coefficient (MCC), as it is better suited for imbalanced problems [52]. Sensitivity and specificity computed at a particular cut-off value are avoided, as they are useless when comparing the performance of different models.

3 Experimental Results

In this section we provide a comprehensive performance analysis of the methodology introduced above.

3.1 Datasets Description

A key aspect of this work is our performance analysis of a wide range of data sources. For each of the considered models, we train them on three different datasets, namely DRIVE [1], CHASE-DB [2] and HRF [3]. The train/validation/test splits for DRIVE are provided by the authors, but there is no official split in the other two cases. We decide to adopt the most restrictive splits we could find in the literature [44]: only 8 of the 22 images in CHASE-DB, and 15 of the 45 images in HRF are used for training and validation.

After training, we test our models on the corresponding test sets. In section 3.3, we also consider another seven different datasets for cross-datasets and domain adaptation evaluation. These include a variety of different image qualities, resolutions, pathologies, and even image modalities. Further details of each of these databases are given in Table 1.

It is also worth mentioning that, for training, all images from DRIVE, CHASEDB, and HRF are downsampled to a 512×512 , 512×512 , and 1024×1024 resolution respectively, whereas evaluation is carried out at native resolution for all datasets. No pre-processing (nor post-processing) was applied.

3.2 Performance Evaluation

For evaluating our approach, we follow the procedure outlined in section 2.5, and report AUC, DICE, and MCC values in Table 2. For comparison purposes, we select a large set of 20 vessel segmentation techniques published in the last years in relevant venues. We also report the performance of a standard U-Net $\phi_{3,8}$, which contains around 34,000 parameters, and our proposed W-Net (with twice as many parameters), referred to as Little U-Net/W-Net.

	Year	# ims.	Resolution	FOV	Challenges & Comments
STARE [4]	2000	20	605×700	35°	Poor quality: scanned and digitized photographs Healthy and pathological images (10/10)
DRIVE [1]	2004	40	565×584	45°	Consistent good quality and contrast, low resolution Mostly healthy patients, some with mild DR (33/40)
CHASE-DB 1 [2]	2012	28	999×960	30°	OD-centered images from 10-year old children Uneven background illumination and poor contrast
HRF [3]	2013	45	3504×2336	60°	High visual quality, images taken with mydriatic dilation Healthy, diabetic, and glaucomatous patients (15/15/15)
DRiDB [9]	2013	50	720×576	45°	Highly varying quality, illumination, and image noise Mostly diabetic patients of varying grades (36/50)
AV-WIDE [8]	2015	30	2816×1880 1500×900	200°	Uneven illumination, varying resolution due to cropping Healthy and age-related macular degeneration patients.
IOSTAR [6]	2016	30	1024×1024	45°	Scanning Laser Ophthalmoscope images Macula-centered, high contrast and visual quality
DR HAGIS [7]	2017	40	2816×1880 4752×3168	45°	Multi-center, multi-device macula-centered images All diabetic patients with different co-morbidities
UoA-DR [10]	2017	200	2124×2056	45°	Both macula and OD-centered images Healthy, NP-DR and P-DR patients (56/114/30)
LES-AV [5]	2018	22	1144×1620 1958×2196	30° 45°	OD-centered images, highly varying illumination 11 healthy and 11 glaucomatous patients

Table 1: Description of each of the ten datasets considered in this paper in terms of image and population characteristics.

As discussed above, not all techniques were trained on the same data splits for the CHASE-DB and HRF datasets. Our splits correspond to those used in [44], which is a model specifically designed to be efficient, and therefore contains a minimal amount of learnable parameters. Surprisingly, we see that the Little U-Net model already surpasses the performance of [44] in all datasets, even if it has 16 times less weights. The performance of the Little U-Net is overall impressive, achieving a performance on-par or superior to most of the compared techniques.

When we analyze the performance of the Little W-Net model, we observe that it surpasses by a wide margin, both in terms of AUC and DICE score, the numbers obtained by all the other techniques. This is specially remarkable when considering that the Little W-Net is a far less complex model than any other approach (excluding Little U-Net). The only dataset where Little W-Net fails to reach the highest performance is HRF, which we attribute to the mismatch in training and test resolutions. The work in [26], which achieves the state-of-the-art in this dataset, was trained on image patches, and it is therefore less susceptible to such mismatch. Nevertheless, the Little W-Net achieves the second best ranking in this dataset, within a short distance from [26].

3.3 Cross-dataset experiments and Domain Adaption

From the above analysis, one could be tempted to conclude that the task of segmenting the vasculature from retinal images is relatively trivial. Nevertheless, the usefulness of these models remains questionable if they are not tested on data coming from sources different than the training data. In order to exhaustively explore this aspect of the problem, we select the W-net model trained on DRIVE images and generate predictions on up to ten different datasets (including the DRIVE test set). We then carry out a performance analysis similar to the one described in section 2.5, and report the results in the first row of Table 3. We can see how the great performance of this model on the DRIVE test set is only maintained on the STARE dataset, which is quite similar in terms of resolution and quality. However, for data arising from different distributions, this performance is rapidly degraded. In terms of AUC, the four worst results correspond to: 1) HRF, which has images of a much greater resolution than DRIVE, 2) LES-AV, where images are centered in the optic disc instead of in the macula, 3) AV-WIDE, which contains ultra-wide field images of markedly different aspect, and 4) UoA-DR, which has mostly pathological images of different resolutions.

We then apply the strategy described in section 2.4: for each dataset we use the model trained on DRIVE to gen-

	# Pub/Year	# Params	DRIVE			CHASE-DB			HRF		
			AUC	DICE	MCC	AUC	DICE	MCC	AUC	DICE	MCC
Maninis <i>et al.</i> [24]	ECCV/2016		—	82.20	—	—	—	—	—	—	—
Zhang <i>et al.</i> [6]	TMI/2016		96.36	—	—	96.06	—	—	96.08	—	74.10
Fu <i>et al.</i> [25]	MICCAI/2016		94.04	78.75	—	94.82	75.49	—	—	—	—
Liskowski <i>et al.</i> [23]	TMI/2016	48,000,000	97.90	—	—	98.45	—	—	—	—	—
Orlando <i>et al.</i> [22]	TBME/2017		95.07	78.57	75.56	95.24	73.32	70.46	95.24	71.58	68.97
Gu <i>et al.</i> [53]	TMI/2017		—	78.86	75.89	—	72.02	69.08	—	77.49	75.41
Wu <i>et al.</i> [54]	MICCAI/2018		98.07	—	—	98.25	—	—	—	—	—
Yan <i>et al.</i> [31]	TBME/2018		97.52	81.83	—	97.81	—	—	—	78.14	—
Wang <i>et al.</i> [55]	BSPC/2019		—	81.44	78.95	—	78.63	76.55	—	—	—
Wang <i>et al.</i> [56]	MICCAI/2019		97.72	82.70	—	98.12	80.37	—	—	—	—
Araujo <i>et al.</i> [57]	MICCAI/2019		97.90	—	—	98.20	—	—	—	—	—
Fu <i>et al.</i> [58]	MICCAI/2019		97.19	80.48	—	—	—	—	—	—	—
Wang <i>et al.</i> [59]	PatRec/2019		—	80.93	78.51	—	78.09	75.91	—	77.31	—
Wu <i>et al.</i> [60]	TMI/2019		97.79	—	—	—	—	—	—	—	—
Zhao <i>et al.</i> [39]	TMI/2019		—	78.82	—	—	—	—	—	76.59	—
Laibacher <i>et al.</i> [44]	CVPR-W/2019	549,748	97.14	80.91	—	97.03	80.06	—	—	78.14	—
Shin <i>et al.</i> [26]	MedIA/2019	7,910,000	98.01	82.63	—	98.30	80.34	—	98.38	81.51	—
Zhao <i>et al.</i> [35]	PatRec/2020		—	82.29	—	—	—	—	—	77.31	—
Zhuo <i>et al.</i> [51]	CMPB/2020		97.54	81.63	—	—	—	—	—	—	—
Mou <i>et al.</i> [34]	TMI/2020	56,030,000	97.96	—	—	98.12	—	—	—	—	—
Little U-Net		34,201	97.98	82.41	79.81	98.22	80.29	78.23	98.11	80.59	78.60
Little W-Net		68,482	98.09	82.82	80.27	98.44	81.55	79.60	98.24	81.04	79.11

Table 2: Performance Comparison of methods trained/tested on DRIVE, CHASE-DB, and HRF. Best results are marked bold.

erate segmentations that we use as pseudo-labels to retrain the same model in an attempt to close the performance gap. Results of this series of experiments are displayed in the second row of Table 3, where it can be seen that in almost all cases this results in an increased performance in terms of AUC, DICE score, and MCC, albeit relatively modest in some datasets. In any case, this implies that the retrained models have a better ability to predict vessel locations on new data. Figure 4 illustrates this for two images sampled from the CHASE-DB and the LES-AV datasets. Note that DRIVE does not contain optic-disc centered images. For the CHASE-DB example, we see that some broken vessels, probably due to the strong central reflex in this image, are recovered with the adapted model. In the LES-AV case, we see how an image with an uneven illumination field results in the DRIVE model missing much of the vessel pixels in the bottom area. Again, part of this vessels are successfully recovered by the adapted model.

3.4 Artery/Vein Segmentation

We also provide results for the related problem of Artery/Vein segmentation. It should be stressed that this is a different task than A/V classification, where the vessel tree is assumed to be available, and the goal is to classify each vessel pixel among the two classes. In this case, we aim to classify each pixel in the entire image as artery, vein, or background. In order to account for

the greater difficulty of the problem, we consider a bigger W-Net composed of two U-Nets $\phi_{4,8}$, which still contains far less weights than current A/V segmentation models [61, 62]. In addition, we double the number of training cycles, and train with 4 classes having into account uncertain pixels, as it has been proven beneficial for this task [61].

Table 4 shows the results of our W-Net, compared with two recent A/V segmentation techniques. In this section, we train our model on DRIVE and HRF, following the data splits provided in [62]. We also show results of a cross-dataset experiment in which a model trained on DRIVE is tested on the LES-AV dataset.

A similar trend as in Section 3.2 can be observed: other models designed for the same task contain orders of magnitude more parameters than our approach, but we observe an excellent performance of the W-Net architecture: it seems competitive with the compared methods, ranking even higher than [62] in terms of Dice score and higher than [61] in terms of MCC, at a fraction of computational cost. Some qualitative results of the W-Net trained on DRIVE and tested on LES-AV are shown in Fig. 5.

3.5 Ablation Study: W-Net vs U-Net

As shown in Section 3.2, the iterative structure of the W-Net architecture helps in achieving a better performance when compared to the standard U-Net. However, it should

	DRIVE			CHASE-DB			HRF			STARE			IOSTAR		
Training Set	AUC	DICE	MCC	AUC	DICE	MCC	AUC	DICE	MCC	AUC	DICE	MCC	AUC	DICE	MCC
DRIVE	98.09	82.82	80.27	97.22	75.13	72.44	95.90	70.39	68.05	98.11	79.48	77.30	97.97	78.77	76.47
PSEUDO-L	98.09	82.82	80.27	97.56	76.49	74.02	96.12	71.12	68.86	98.28	79.76	77.65	98.06	78.95	76.73

	DRiDB			LES-AV			DR HAGIS			AV-WIDE			UoA-DR		
Training Set	AUC	DICE	MCC	AUC	DICE	MCC	AUC	DICE	MCC	AUC	DICE	MCC	AUC	DICE	MCC
DRIVE	96.17	68.45	66.62	95.45	76.60	74.32	97.17	67.92	66.79	86.54	61.51	59.02	82.32	38.29	35.51
PSEUDO-L	96.52	68.25	66.59	97.34	77.93	75.92	97.34	68.67	67.49	87.64	62.46	59.97	82.71	37.68	34.97

Table 3: Our domain adaptation strategy improves results in a wide range of external test sets. First row: W-Net trained on DRIVE, second row (pseudo-l): same model fine-tuned using the strategy illustrated in Fig. 3. Best metric marked bold.



Figure 4: The Domain Adaptation strategy from section 2.4 recovers some missing vessels. Segmentations produced by a model trained on DRIVE (which contains macula-centered images) when using data from CHASE-DB and LES-AV (which contain OD-centered images). In (a) and (b), the retinal image (left), the segmentation by the model trained on DRIVE (center) and the one produced by the model trained on pseudo-labels (right).

be noted that W-Net contains twice as many weights as the considered Little U-Net. Since these are two relatively small models, it might be that U-Net is simply underfitting, and all the benefits observed in Table 2 just come from doubling the parameters and not from any algorithmic improvement.

In view of this, it is worth investigating the question of whether W-Net brings a significant improvement over a standard U-Net architecture. For this, we consider a larger U-Net $\phi_{3,12}$, which actually contains more parameters than the above W-Net (76K vs 68K). To determine statistically significant differences in AUC and DICE between these two models, we train them under the exact same conditions as in Section 3.2, and after generating the corresponding predicted segmentations on each of the three test sets, we apply the bootstrap procedure as in [63, 64]. This is, each test set is randomly sampled with replacement 100 times so that each new set of sampled data contains the same number of examples as the original set, in the same proportion of vessel/background pixels. For both models, we calculate the differences in AUCs and dice scores. Resampling 100 times results in 100 values for performance differences. P-values are defined as the fraction of values that are negative or zero, corresponding to cases in which the better model in each dataset performed worse or equally than the other model. The statistical significance level is set to 5% and, thus, performance differences are considered statistically sig-

nificant if $p < 0.05$. The resulting performance differences are reported in Table 5, where we refer to the U-Net $\phi_{3,12}$ as “Big U-Net”. We see that, in all cases, the larger U-Net’s results are slightly better than the smaller U-Net in Table 2, but the performance of the W-Net is still significantly higher, even if it has approximately 10% less weights.

3.6 Computational and Memory Requirements

The reduced complexity of the models proposed in this paper enhance their suitability for resource-constrained scenarios, both in terms of training them and of deploying them in, e.g., portable devices. Training a little U-Net and a little W-Net to reach the performance shown in Table 2 is feasible even without a GPU. When training on a single GPU (GeForce RTX 2080 Ti), the training time of a little U-Net on the datasets shown in Table 2 was 24 mins (DRIVE), 22 mins (CHASE-DB) and 102 mins (HRF), whereas the little W-Net took 32 mins (DRIVE), 30 mins (CHASE-DB) and 140 mins (HRF). Regarding disk memory requirements, Table 6 shows a comparison of both architectures with another two popular models in terms of performance vs. number of parameters/disk size. We see that a little U-Net, which already attains a great performance, has the lowest disk storage space (161Kb), and the top-performant W-Net takes approximately twice this space, which is still well within limits for its deployment

	# Params	DRIVE		HRF		LES-AV*	
		DICE	MCC	DICE	MCC	DICE	MCC
[61]	~29M	96.31 96.25	74.79 25.07	—	—	96.59	70.58
[62]	~5M	96.71 95.81	77.57 24.67	96.88	76.89	—	—
W-Net	~279K	96.69 95.55	77.73 25.23	96.89	76.19	96.46	70.30

Table 4: Performance Comparison for the artery/vein segmentation task. For DRIVE, performance is reported on the entire image domain | on a ring-shaped region around the Optic Disc [62]. Performance is computed using the predictions and code provided by [62]. *Predictions on LES-AV are generated from models trained on DRIVE.

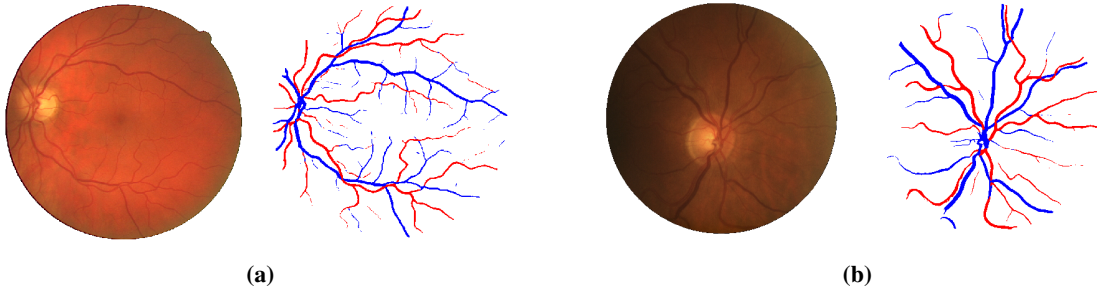


Figure 5: Generalization ability of a W-Net trained for A/V segmentation. Results of our model trained on DRIVE and tested on (a) DRIVE, (b) LES-AV.

in embedded/portable devices. It must be noted, however, that in both cases the inference time was slightly slower when compare to other efficient approaches, partly due to implementation of Test-Time Augmentation.

4 Conclusions

This paper reflects on the need of constructing algorithmically complex methodologies for the task of retinal vessel segmentation. In a quest for squeezing an extra drop of performance on public benchmark datasets and adding certain novelty, recent works on this topic show a trend to develop overcomplicated pipelines that may not be necessary for this task. The first conclusion to be drawn from our work is that sometimes Occam’s razor works best:

minimalistic models, properly trained, can attain results that do not significantly differ from what one can achieve with more complex approaches.

Another point worth stressing is the need of rigor in evaluating retinal vessel segmentation techniques. Employing overly favorable train/test splits or incorrectly computing performance leads to reporting inflated metrics, which in turn saturate public benchmarks and provides a false sensation in the community that the retinal vessel segmentation problem is solved. Our experiments on a wide range of datasets reveal that this is not the case, and that retinal vessel segmentation is indeed an ideal area for experimenting with domain adaptation techniques. This is so because a) performance of models trained on a source dataset rapidly degrades when testing on a different kind

	# Params	DRIVE		CHASE-DB		HRF	
		AUC	DICE	AUC	DICE	AUC	DICE
“Big” U-Net	76,213	98.00	82.53	98.29	81.09	98.15	80.73
Little W-Net	68,482	98.09	82.78	98.44	81.52	98.24	81.05
W-Net vs U-Net	-7,731	+0.09 p<0.05	+0.25 p<0.05	+0.15 p<0.05	+0.43 p<0.05	+0.09 p<0.05	+0.32 p<0.05

Table 5: Performance comparison between a W-Net and a U-Net configured to have a comparable amount of weights. W-Net achieves higher performance, despite having slightly less parameters. Statistically significant results marked bold.

	# Params	Size	DRIVE		CHASEDB		HRF	
			AUC	DICE	AUC	DICE	AUC	DICE
DRIU [24]	15M	57Mb	n/a	82.20	n/a	n/a	n/a	n/a
M2U-Net [44]	0.5M	2.2Mb	97.14	80.91	97.03	80.06	n/a	78.14
Little U-Net	34K	161Kb	97.98	82.41	98.22	80.68	98.11	80.59
Little W-Net	68K	325Kb	98.09	82.82	98.44	81.55	98.24	81.04

Table 6: Parameters and memory requirements vs performance for several retinal vessel segmentation models.

of data, and b) training models to achieve high performance is cheap and fast, which enables fast experimentation of new ideas.

References

- [1] J. Staal, M.D. Abramoff, M. Niemeijer, M.A. Viergever, and B. van Ginneken. Ridge-based vessel segmentation in color images of the retina. *IEEE Transactions on Medical Imaging*, 23(4):501–509, April 2004.
- [2] Muhammad Moazam Fraz, Paolo Remagnino, Andreas Hoppe, Bunyarit Uyyanonvara, Alicja R. Rudnicka, Christopher G. Owen, and Sarah A. Barman. An Ensemble Classification-Based Approach Applied to Retinal Blood Vessel Segmentation. *IEEE Transactions on Biomedical Engineering*, 59(9):2538–2548, September 2012.
- [3] A. Budai, R. Bock, A. Maier, J. Hornegger, and G. Michelson. Robust Vessel Segmentation in Fundus Images. *International Journal of Biomedical Imaging*, 2013:154860, December 2013.
- [4] A.D. Hoover, V. Kouznetsova, and M. Goldbaum. Locating blood vessels in retinal images by piecewise threshold probing of a matched filter response. *IEEE Transactions on Medical Imaging*, 19(3):203–210, March 2000.
- [5] José Ignacio Orlando, João Barbosa Breda, Karel van Keer, Matthew B. Blaschko, Pablo J. Blanco, and Carlos A. Bulant. Towards a Glaucoma Risk Index Based on Simulated Hemodynamics from Fundus Images. In Alejandro F. Frangi, Julia A. Schnabel, Christos Davatzikos, Carlos Alberola-López, and Gabor Fichtinger, editors, *Medical Image Computing and Computer Assisted Intervention – MICCAI 2018*, Lecture Notes in Computer Science, pages 65–73, Cham, 2018. Springer International Publishing.
- [6] Jiong Zhang, Behdad Dashtbozorg, Erik Bekkers, Josien P. W. Pluim, Remco Duits, and Bart M. ter Haar Romeny. Robust Retinal Vessel Segmentation via Locally Adaptive Derivative Frames in Orientation Scores. *IEEE Transactions on Medical Imaging*, 35(12):2631–2644, December 2016.
- [7] Sven Holm, Greg Russell, Vincent Nourrit, and Niall McLoughlin. DR HAGIS—a fundus image database for the automatic extraction of retinal surface vessels from diabetic patients. *Journal of Medical Imaging (Bellingham, Wash.)*, 4(1):014503, January 2017.
- [8] Rolando Estrada, Michael J. Allingham, Priyatham S. Mettu, Scott W. Cousins, Carlo Tomasi, and Sina Farsiu. Retinal artery-vein classification via topology estimation. *IEEE transactions on medical imaging*, 34(12):2518–2534, December 2015.
- [9] Pavle Prentašić, Sven Lončarić, Zoran Vatavuk, Goran Benčić, Marko Subašić, Tomislav Petković, Lana Dujmović, Maja Malenica-Ravlić, Nikolina Budimlija, and Rašeljka Tadić. Diabetic retinopathy image database(DRiDB): A new database for diabetic retinopathy screening programs research. In *2013 8th International Symposium on Image and Signal Processing and Analysis (ISPA)*, pages 711–716, September 2013. ISSN: 1845-5921.
- [10] Renoh Johnson Chalakkal, Waleed H. Abdulla, and S. Sinumol. Comparative Analysis of University of Auckland Diabetic Retinopathy Database. In *Proceedings of the 9th International Conference on Signal Processing Systems, ICSPS 2017*, pages 235–239, Auckland, New Zealand, November 2017. Association for Computing Machinery.
- [11] Meindert Niemeijer, Xiayu Xu, Alina V. Dumitrescu, Priya Gupta, Bram van Ginneken, James C. Folk, and Michael D. Abramoff. Automated Measurement of the Arteriolar-to-Venular Width Ratio in Digital Color Fundus Photographs. *IEEE Transactions on Medical Imaging*, 30(11):1941–1950, November 2011.
- [12] R. A. Welikala, M. M. Fraz, P. J. Foster, P. H. Whincup, A. R. Rudnicka, C. G. Owen, D. P. Strachan, and S. A. Barman. Automated retinal image quality assessment on the UK Biobank dataset for epidemiological studies. *Computers in Biology and Medicine*, 71:67–76, April 2016.
- [13] Li Chen, Xiaotong Huang, and Jing Tian. Retinal image registration using topological vascular tree segmentation and bifurcation structures. *Biomedical Signal Processing and Control*, 16:22–31, February 2015.

- [14] Pedro Costa, Adrian Galdran, Maria Ines Meyer, Meindert Niemeijer, Michael Abràmoff, Ana Maria Mendonça, and Aurélio Campilho. End-to-End Adversarial Retinal Image Synthesis. *IEEE Transactions on Medical Imaging*, 37(3):781–791, March 2018.
- [15] F. Zana and J.-C. Klein. Segmentation of vessel-like patterns using mathematical morphology and curvature evaluation. *IEEE Transactions on Image Processing*, 10(7):1010–1019, July 2001.
- [16] A.M. Mendonca and A. Campilho. Segmentation of retinal blood vessels by combining the detection of centerlines and morphological reconstruction. *IEEE Transactions on Medical Imaging*, 25(9):1200–1213, September 2006.
- [17] Alejandro F. Frangi, Wiro J. Niessen, Koen L. Vincken, and Max A. Viergever. Multiscale vessel enhancement filtering. In William M. Wells, Alan Colchester, and Scott Delp, editors, *Medical Image Computing and Computer-Assisted Intervention – MICCAI’98*, Lecture Notes in Computer Science, pages 130–137, Berlin, Heidelberg, 1998. Springer.
- [18] George Azzopardi, Nicola Strisciuglio, Mario Vento, and Nicolai Petkov. Trainable COSFIRE filters for vessel delineation with application to retinal images. *Medical Image Analysis*, 19(1):46–57, January 2015.
- [19] J.V.B. Soares, J.J.G. Leandro, R.M. Cesar, H.F. Jelinek, and M.J. Cree. Retinal vessel segmentation using the 2-D Gabor wavelet and supervised classification. *IEEE Transactions on Medical Imaging*, 25(9):1214–1222, September 2006.
- [20] Diego Marín, Arturo Aquino, Manuel Emilio Gegundez-Arias, and José Manuel Bravo. A New Supervised Method for Blood Vessel Segmentation in Retinal Images by Using Gray-Level and Moment Invariants-Based Features. *IEEE Transactions on Medical Imaging*, 30(1):146–158, January 2011.
- [21] Carlos Becker, Roberto Rigamonti, Vincent Lepetit, and Pascal Fua. Supervised Feature Learning for Curvilinear Structure Segmentation. In Kensaku Mori, Ichiro Sakuma, Yoshinobu Sato, Christian Barillot, and Nassir Navab, editors, *Medical Image Computing and Computer-Assisted Intervention – MICCAI 2013*, Lecture Notes in Computer Science, pages 526–533, Berlin, Heidelberg, 2013. Springer.
- [22] Jose Ignacio Orlando, Elena Prokofyeva, and Matthew B. Blaschko. A Discriminatively Trained Fully Connected Conditional Random Field Model for Blood Vessel Segmentation in Fundus Images. *IEEE transactions on bio-medical engineering*, 64(1):16–27, 2017.
- [23] Paweł Liskowski and Krzysztof Krawiec. Segmenting Retinal Blood Vessels With Deep Neural Networks. *IEEE Transactions on Medical Imaging*, 35(11):2369–2380, November 2016.
- [24] Kevis-Kokitsi Maninis, Jordi Pont-Tuset, Pablo Arbeláez, and Luc Van Gool. Deep Retinal Image Understanding. In Sebastien Ourselin, Leo Joskowicz, Mert R. Sabuncu, Gozde Unal, and William Wells, editors, *Medical Image Computing and Computer-Assisted Intervention – MICCAI 2016*, Lecture Notes in Computer Science, pages 140–148, Cham, 2016. Springer International Publishing.
- [25] Huazhu Fu, Yanwu Xu, Stephen Lin, Damon Wing Kee Wong, and Jiang Liu. DeepVessel: Retinal Vessel Segmentation via Deep Learning and Conditional Random Field. In Sebastien Ourselin, Leo Joskowicz, Mert R. Sabuncu, Gozde Unal, and William Wells, editors, *Medical Image Computing and Computer-Assisted Intervention – MICCAI 2016*, Lecture Notes in Computer Science, pages 132–139, Cham, 2016. Springer International Publishing.
- [26] Seung Yeon Shin, Soochahn Lee, Il Dong Yun, and Kyoung Mu Lee. Deep vessel segmentation by learning graphical connectivity. *Medical Image Analysis*, 58:101556, December 2019.
- [27] Yanfei Guo and Yanjun Peng. BSCN: bidirectional symmetric cascade network for retinal vessel segmentation. *BMC Medical Imaging*, 20(1):20, February 2020.
- [28] Zhun Fan, Jiajie Mo, Benzhang Qiu, Wenji Li, Guijie Zhu, Chong Li, Jianye Hu, Yibiao Rong, and Xinjian Chen. Accurate Retinal Vessel Segmentation via Octave Convolution Neural Network. *arXiv:1906.12193 [cs, eess]*, August 2019. arXiv: 1906.12193.
- [29] Kun Wang, Xiaohong Zhang, Sheng Huang, Qiuli Wang, and Feiyu Chen. CTF-Net: Retinal Vessel Segmentation via Deep Coarse-To-Fine Supervision Network. In *2020 IEEE 17th International Symposium on Biomedical Imaging (ISBI)*, pages 1237–1241, April 2020. ISSN: 1945-8452.
- [30] Venkateswararao Cherukuri, Vijay Kumar B.G., Raja Bala, and Vishal Monga. Deep Retinal Image Segmentation With Regularization Under Geometric Priors. *IEEE Transactions on Image Processing*, 29:2552–2567, 2020.
- [31] Zengqiang Yan, Xin Yang, and Kwang-Ting Cheng. Joint Segment-Level and Pixel-Wise Losses for Deep Learning Based Retinal Vessel Segmentation. *IEEE Transactions on Biomedical Engineering*, 65(9):1912–1923, September 2018.
- [32] Olaf Ronneberger, Philipp Fischer, and Thomas Brox. U-Net: Convolutional Networks for Biomedical Image Segmentation. In Nassir Navab, Joachim Hornegger, William M. Wells, and Alejandro F. Frangi, editors, *Medical Image Computing and Computer-Assisted Intervention – MICCAI 2015*, Lecture Notes in Computer Science, pages 234–241, Cham, 2015. Springer International Publishing.

- [33] Zengqiang Yan, Xin Yang, and Kwang-Ting Cheng. A Three-Stage Deep Learning Model for Accurate Retinal Vessel Segmentation. *IEEE Journal of Biomedical and Health Informatics*, 23(4):1427–1436, July 2019.
- [34] Lei Mou, Li Chen, Jun Cheng, Zaiwang Gu, Yitian Zhao, and Jiang Liu. Dense Dilated Network With Probability Regularized Walk for Vessel Detection. *IEEE Transactions on Medical Imaging*, 39(5):1392–1403, May 2020.
- [35] He Zhao, Huiqi Li, and Li Cheng. Improving retinal vessel segmentation with joint local loss by matting. *Pattern Recognition*, 98:107068, February 2020.
- [36] Yishuo Zhang and Albert C. S. Chung. Deep Supervision with Additional Labels for Retinal Vessel Segmentation Task. In Alejandro F. Frangi, Julia A. Schnabel, Christos Davatzikos, Carlos Alberola-López, and Gabor Fichtinger, editors, *Medical Image Computing and Computer Assisted Intervention – MICCAI 2018*, Lecture Notes in Computer Science, pages 83–91, Cham, 2018. Springer International Publishing.
- [37] Avisek Lahiri, Kumar Ayush, Prabir Kumar Biswas, and Pabitra Mitra. Generative Adversarial Learning for Reducing Manual Annotation in Semantic Segmentation on Large Scale Microscopy Images: Automated Vessel Segmentation in Retinal Fundus Image as Test Case. pages 42–48, 2017.
- [38] Jaemin Son, Sang Jun Park, and Kyu-Hwan Jung. Towards Accurate Segmentation of Retinal Vessels and the Optic Disc in Fundoscopic Images with Generative Adversarial Networks. *Journal of Digital Imaging*, 32(3):499–512, June 2019.
- [39] He Zhao, Huiqi Li, Sebastian Maurer-Stroh, Yuhong Guo, Qiuju Deng, and Li Cheng. Supervised Segmentation of Un-Annotated Retinal Fundus Images by Synthesis. *IEEE Transactions on Medical Imaging*, 38(1):46–56, January 2019.
- [40] Kyeong-Beom Park, Sung Ho Choi, and Jae Yeol Lee. M-GAN: Retinal Blood Vessel Segmentation by Balancing Losses through Stacked Deep Fully Convolutional Networks. *IEEE Access*, pages 1–1, 2020.
- [41] Francisco Argüello, David L. Vilariño, Dora B. Heras, and Alejandro Nieto. GPU-based segmentation of retinal blood vessels. *Journal of Real-Time Image Processing*, 14(4):773–782, April 2018.
- [42] Pedro Bibiloni, Manuel González-Hidalgo, and Sebastia Massanet. A real-time fuzzy morphological algorithm for retinal vessel segmentation. *Journal of Real-Time Image Processing*, 16(6):2337–2350, December 2019.
- [43] Xiayu Xu, Wenxiang Ding, Xuemin Wang, Ruofan Cao, Maiye Zhang, Peilin Lv, and Feng Xu. Smartphone-Based Accurate Analysis of Retinal Vasculature towards Point-of-Care Diagnostics. *Scientific Reports*, 6(1):34603, October 2016.
- [44] Tim Laibacher, Tillman Weyde, and Sepehr Jalali. M2U-Net: Effective and Efficient Retinal Vessel Segmentation for Real-World Applications. In *2019 IEEE/CVF Conference on Computer Vision and Pattern Recognition Workshops (CVPRW)*, pages 115–124, June 2019. ISSN: 2160-7516.
- [45] Mark Sandler, Andrew G. Howard, Menglong Zhu, Andrey Zhmoginov, and Liang-Chieh Chen. MobileNetV2: Inverted Residuals and Linear Bottlenecks. *2018 IEEE/CVF Conference on Computer Vision and Pattern Recognition*, pages 4510–4520, 2018.
- [46] Wei-Yu Chen, Yen-Cheng Liu, Zsolt Kira, Yu-Chiang Wang, and Jia-Bin Huang. A Closer Look at Few-shot Classification. In *International Conference on Learning Representations*, 2019.
- [47] Kevin Musgrave, Serge Belongie, and Ser-Nam Lim. A Metric Learning Reality Check. In *European Conference on Computer Vision*, July 2020. arXiv: 2003.08505.
- [48] Wouter Marco Kouw and Marco Loog. A review of domain adaptation without target labels. *IEEE Transactions on Pattern Analysis and Machine Intelligence*, pages 1–1, 2019.
- [49] Américo Oliveira, Sérgio Pereira, and Carlos A. Silva. Retinal vessel segmentation based on Fully Convolutional Neural Networks. *Expert Systems with Applications*, 112:229–242, December 2018.
- [50] Xiayu Xu, Wenxiang Ding, Michael D. Abramoff, and Ruofan Cao. An improved arteriovenous classification method for the early diagnostics of various diseases in retinal image. *Computer Methods and Programs in Biomedicine*, 141:3–9, April 2017.
- [51] Zhongshuo Zhuo, Jianping Huang, Ke Lu, Daru Pan, and Shouting Feng. A size-invariant convolutional network with dense connectivity applied to retinal vessel segmentation measured by a unique index. *Computer Methods and Programs in Biomedicine*, 196:105508, November 2020.
- [52] Davide Chicco and Giuseppe Jurman. The advantages of the Matthews correlation coefficient (MCC) over F1 score and accuracy in binary classification evaluation. *BMC Genomics*, 21(1):6, January 2020.
- [53] Lin Gu, Xiaowei Zhang, He Zhao, Huiqi Li, and Li Cheng. Segment 2D and 3D Filaments by Learning Structured and Contextual Features. *IEEE Transactions on Medical Imaging*, 36(2):596–606, February 2017.
- [54] Yicheng Wu, Yong Xia, Yang Song, Yanning Zhang, and Weidong Cai. Multiscale Network Followed Network Model for Retinal Vessel Segmentation. In Alejandro F. Frangi, Julia A. Schnabel, Christos Davatzikos, Carlos Alberola-López, and Gabor

- Fichtinger, editors, *Medical Image Computing and Computer Assisted Intervention – MICCAI 2018*, Lecture Notes in Computer Science, pages 119–126, Cham, 2018. Springer International Publishing.
- [55] Xiaohong Wang and Xudong Jiang. Retinal vessel segmentation by a divide-and-conquer funnel-structured classification framework. *Signal Processing*, 165:104–114, December 2019.
- [56] Bo Wang, Shuang Qiu, and Huiguang He. Dual Encoding U-Net for Retinal Vessel Segmentation. In Dinggang Shen, Tianming Liu, Terry M. Peters, Lawrence H. Staib, Caroline Essert, Sean Zhou, Pew-Thian Yap, and Ali Khan, editors, *Medical Image Computing and Computer Assisted Intervention – MICCAI 2019*, Lecture Notes in Computer Science, pages 84–92, Cham, 2019. Springer International Publishing.
- [57] Ricardo J. Araújo, Jaime S. Cardoso, and Hélder P. Oliveira. A Deep Learning Design for Improving Topology Coherence in Blood Vessel Segmentation. In Dinggang Shen, Tianming Liu, Terry M. Peters, Lawrence H. Staib, Caroline Essert, Sean Zhou, Pew-Thian Yap, and Ali Khan, editors, *Medical Image Computing and Computer Assisted Intervention – MICCAI 2019*, Lecture Notes in Computer Science, pages 93–101, Cham, 2019. Springer International Publishing.
- [58] Weilin Fu, Katharina Breininger, Roman Schaffert, Nishant Ravikumar, and Andreas Maier. A Divide-and-Conquer Approach Towards Understanding Deep Networks. In Dinggang Shen, Tianming Liu, Terry M. Peters, Lawrence H. Staib, Caroline Essert, Sean Zhou, Pew-Thian Yap, and Ali Khan, editors, *Medical Image Computing and Computer Assisted Intervention – MICCAI 2019*, Lecture Notes in Computer Science, pages 183–191, Cham, 2019. Springer International Publishing.
- [59] Xiaohong Wang, Xudong Jiang, and Jianfeng Ren. Blood vessel segmentation from fundus image by a cascade classification framework. *Pattern Recognition*, 88:331–341, April 2019.
- [60] Zaiwang Gu, Jun Cheng, Huazhu Fu, Kang Zhou, Huaying Hao, Yitian Zhao, Tianyang Zhang, Shenghua Gao, and Jiang Liu. CE-Net: Context Encoder Network for 2D Medical Image Segmentation. *IEEE Transactions on Medical Imaging*, 38(10):2281–2292, October 2019.
- [61] Adrian Galdran, M. Meyer, P. Costa, Mendonça, and A. Campilho. Uncertainty-Aware Artery/Vein Classification on Retinal Images. In *2019 IEEE 16th International Symposium on Biomedical Imaging (ISBI 2019)*, pages 556–560, April 2019. ISSN: 1945-8452.
- [62] Ruben Hemelings, Bart Elen, Ingeborg Stalmans, Karel Van Keer, Patrick De Boever, and Matthew B. Blaschko. Artery–vein segmentation in fundus images using a fully convolutional network. *Computerized Medical Imaging and Graphics*, 76:101636, September 2019.
- [63] F.W. Samuelson and N. Petrick. Comparing image detection algorithms using resampling. In *3rd IEEE International Symposium on Biomedical Imaging: Nano to Macro, 2006.*, pages 1312–1315, April 2006. ISSN: 1945-8452.
- [64] Alessandro Bria, Claudio Marrocco, and Francesco Tortorella. Addressing class imbalance in deep learning for small lesion detection on medical images. *Computers in Biology and Medicine*, 120:103735, May 2020.